DOI: 10.1002/anie.201203849

Spectroscopic Methods

Nanoscale Chemical Imaging Using Tip-Enhanced Raman Spectroscopy: A Critical Review

*Thomas Schmid, Lothar Opilik, Carolin Blum, and Renato Zenobi**

Keywords:
nanoscale analysis · Raman spectroscopy · scanning probe microscopy · spectroscopic imaging · tip-enhanced Raman-spectroscopy (TERS)

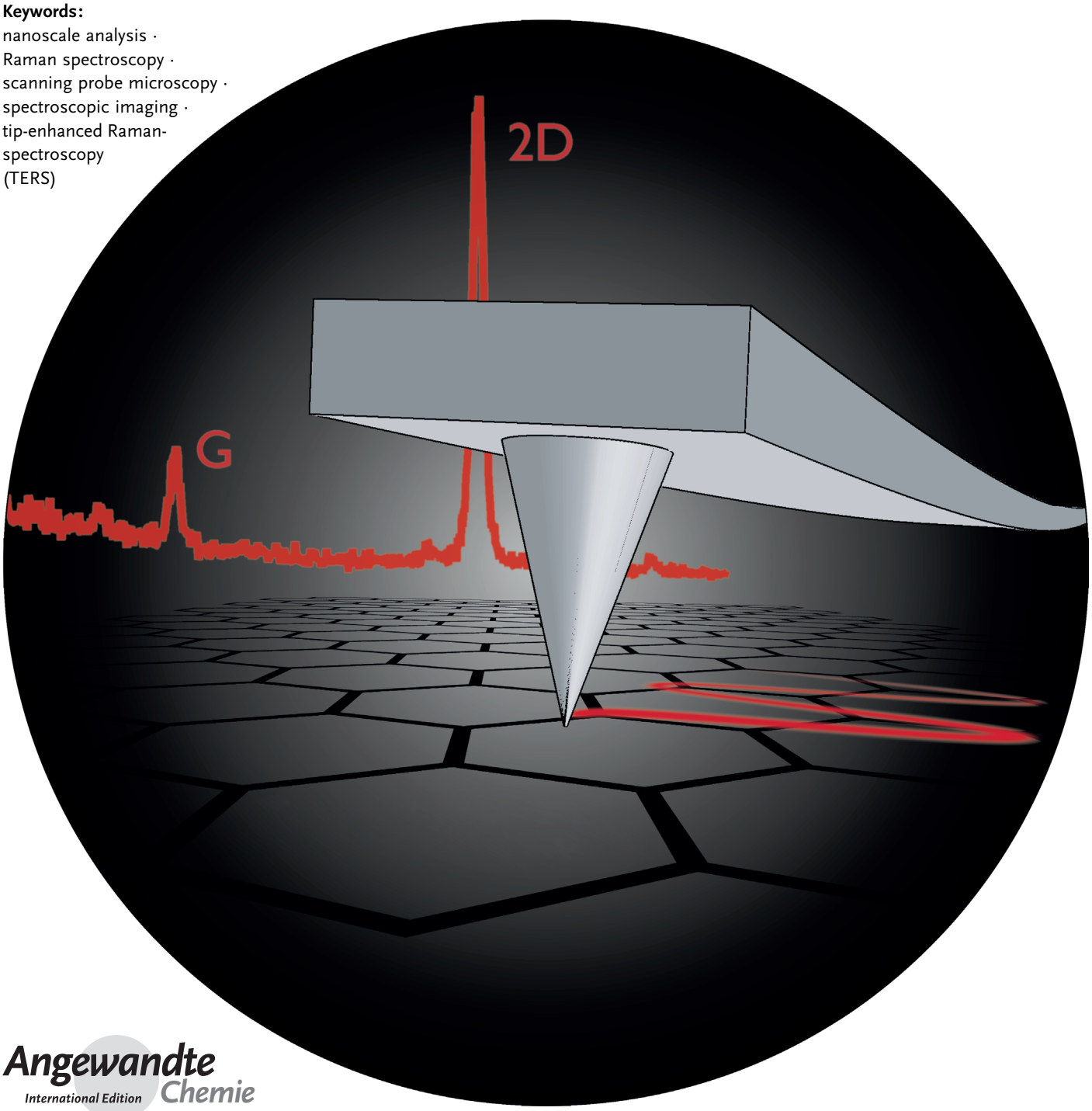

Angewandte International Edition Chemie

Methods for chemical analysis at the nanometer scale are crucial for understanding and characterizing nanostructures of modern materials and biological systems. Tip-enhanced Raman spectroscopy (TERS) combines the chemical information provided by Raman spectroscopy with the signal enhancement known from surface-enhanced Raman scattering (SERS) and the high spatial resolution of atomic force microscopy (AFM) or scanning tunneling microscopy (STM). A metallic or metallized tip is illuminated by a focused laser beam and the resulting strongly enhanced electromagnetic field at the tip apex acts as a highly confined light source for Raman spectroscopic measurements. This Review focuses on the prerequisites for the efficient coupling of light to the tip as well as the shortcomings and pitfalls that have to be considered for TERS imaging, a fascinating but still challenging way to look at the nanoworld. Finally, examples from recent publications have been selected to demonstrate the potential of this technique for chemical imaging with a spatial resolution of approximately 10 nm and sensitivity down to the single-molecule level for applications ranging from materials sciences to life sciences.

From the Contents

1. Introduction

Molecular analysis on the nanoscale is becoming more and more important due to advances and new challenges in areas such as heterogeneous catalysis, molecular electronics, biophysics, and biology. Methods that provide insight into the nanoscale are, for example, electron microscopy (EM), scanning probe microscopy (SPM, such as atomic force microscopy, AFM, and scanning tunneling microscopy, STM), as well as modern super-resolving fluorescence microscopy methods (stochastic optical reconstruction microscopy, STORM, stimulated emission depletion, STED, and photoactivated localization microscopy, PALM).[1–6] However, these methods have limitations: some of them do not yield any molecular/spectroscopic information (EM, STM, AFM), while others require labeling (PALM, STORM, and some EM techniques). Ideally, one would like to be able to investigate complex, heterogeneous samples:

- with a method that can identify compounds based on their spectroscopic fingerprint;
- in a label-free fashion;
- with a spatial resolution down to a few nm;
- with a method capable of simultaneous topographic and spectroscopic imaging;
- with a sensitivity approaching that of a few molecules.

Tip-enhanced Raman spectroscopy (TERS) comes close to fulfilling all of these demands. Developed a bit over a decade ago,[7–10] TERS is the spectroscopic "cousin" of AFM and STM, and originated as an "apertureless" version[11] of scanning near-field optical microscopy (SNOM). It is a near-field optical technique in which a metal or metallized SPM tip is illuminated with a focused, diffraction-limited excitation beam. The tip can be scanned across a sample surface and acts as a near-field light source (Figure 1). The principle of TERS is related to surface-enhanced Raman scattering (SERS),

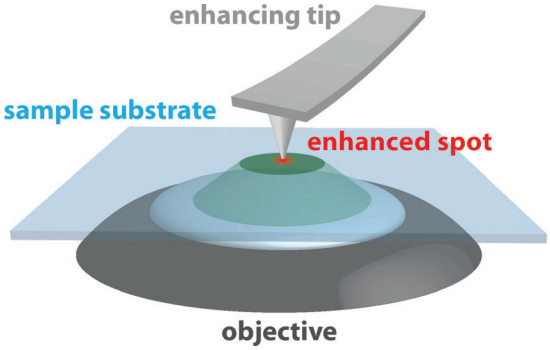

Figure 1. Typical TERS setup with bottom illumination and a metallized AFM tip to provide local field enhancement. The objective is used to focus the excitation beam (green) onto the sample surface and to collect the Raman scattered light. Enhanced Raman scattering originates from a small fraction of the illuminated area (red) where the TERS tip is in close proximity to the sample surface.

where metallic nanoparticles or nanostructures lead to a large enhancement of the normally weak Raman signal of adsorbed analyte molecules by several orders of magnitude.[12] The main difference is that in TERS the enhancement only originates from one single enhancing metallic nanostructure at the end of an SPM tip, whereas in SERS many different enhancing "hot spots" are present and lead to an averaged spectrum. Although often desired in SERS, the adsorption of analyte molecules to the enhancing structure should be prevented in TERS. The SPM part of a TERS instrument

[*] T. Schmid, L. Opilik,[+] C. Blum,[+] R. Zenobi
Department of Chemistry and Applied Biosciences
ETH Zürich
CH-8093 Zürich (Switzerland)
E-mail: zenobi@org.chem.ethz.ch
[+] These authors contributed equally to this work.

allows the nanometer-sized light source to be placed at specific positions on the sample or—by raster scanning either the sample or the tip—performing imaging experiments with the full spectroscopic information collected at every pixel. TERS is on the verge of becoming more widespread, partly because manufacturers of scanning probe microscopes are beginning to make serious efforts to design TERS instruments and fabricate reliable TERS tips, partly because there is a real need in many areas of science and technology to obtain detailed molecular information with high spatial resolution. The recent advances to establish TERS as a high-resolution imaging technique are particularly promising. This Review will, therefore, focus on the challenges and recent applications of TERS imaging.

We begin with a discussion on the prerequisites for efficient optical coupling of incident light to the TERS tip (Section 2). We critically address important issues in TERS imaging, such as correct band assignments for complex (biological) samples as well as tip contamination and degradation, as TERS users must also be aware of the shortcomings and pitfalls of this method (Section 3). Finally, we discuss some recent examples from the literature to demonstrate how TERS can visualize the molecular distribution of complex samples, for example, nanotubes, graphene, solar cell materials, and supported lipid layers as models for cell membranes (Section 4).

2. Near-Field Optical Probes

Since the very beginning of SNOM, the production and characterization of tips/probes for near-field optical methods have always been a key factor in deciding the success or failure of such experiments. SNOM first existed as a thought experiment by Synge, who in 1928 proposed to bring a very small aperture (with a size well below the optical diffraction limit) very close to a sample surface.[13] The illuminated aperture would thus act as a near-field light source to obtain images with subdiffraction spatial resolution when scanning it across the sample surface. 56 years after publication of this general idea, the experimental realization with visible light was accomplished by using a metal-coated glass-fiber tip with a small aperture at its apex.[14,15] However, because the light intensity decreases significantly when reducing the physical size of the aperture, the best spatial resolution obtained so far with this approach is in the range of 50 nm.[16] A spatial resolution higher than that is desirable in many different areas of research and technology. With apertureless SNOM (called TERS when used for Raman spectroscopic measurements) a spatial resolution down to 4 nm has been demonstrated experimentally.[11] The key difference compared to aperture SNOM is that instead of a subdiffraction aperture, a nanometer-sized scatterer illuminated with a diffraction-limited light source is scanned across the sample surface. The tiny scatterer can lead to an enhanced optical field in its proximity (mainly arising from localized surface plasmon resonances), and thereby acts as a near-field light source. The main drawback accompanying this approach is the background signal resulting from the necessary far-field illumination. However, different approaches have been presented in the literature to remove or suppress this far-field contribution.[17–20] Another issue of TERS that has not been solved so far is that suitable optical probes cannot yet be fabricated reproducibly. Etched metal wires or metal-coated SPM probes are easy to produce and are commonly used, but lack reproducibility.

The main factors that influence the efficient coupling of light to an optical probe are the tip geometry, its material and dielectric function $\varepsilon(\omega)$, the dielectric constant ε_M of the materials surrounding the tip, as well as the angle of incidence and the polarization of the incident light. As a very simple first approximation, the tip apex can be considered a small sphere with a size much smaller than the excitation wavelength (and smaller than the skin depth of the metal). In this case, the electrostatic (or quasistatic) approximation is valid and the internal electric field E_{in} is described by an electric dipole in the center of the sphere.[21] The ratio of the internal electric field E_{in} to the incident field strength E_0 becomes very large if $\varepsilon(\omega) \approx -2\varepsilon_M$, i.e., when $\mathrm{Im}(\varepsilon(\omega))$ is close to zero and $\mathrm{Re}(\varepsilon(\omega))$ is close to $-2\varepsilon_M$.[12] This is only possible for materials having values of $\mathrm{Re}(\varepsilon(\omega))$ between -1 and -20 in the frequency range of interest.[12] The condition $\varepsilon(\omega) \approx -2\varepsilon_M$ leads to a strong optical response only at a certain (resonance) frequency ω. This is a simple example of a localized surface plasmon resonance that specifies the required wavelength at which the most efficient coupling to the optical probe will occur. Materials with the required optical properties exist and can be identified after evaluation of their dielectric functions.

Thomas Schmid was born in Bolzano (Italy). He received his Diploma in Chemistry in 1999 and his PhD in 2003 from the Technische Universität München (Germany). In 2005, he joined the ETH Zurich as a fellow of the German Research Foundation (DFG), and has been a senior research associate and lecturer there since 2007. His research interests include nanoscale chemical analysis and chemical imaging using tip-enhanced Raman spectroscopy (TERS) as well as general combinations of AFM/STM and Raman microscopy, with a focus on method development and applications in biology and materials science.

Lothar Opilik studied chemistry at the ETH Zurich (M.Sc. 2009). He carried out his master thesis in the research group of Prof. Reinhard Niessner at the TU Munich. He then returned to Zurich in 2009 to start PhD studies in the group of Prof. Renato Zenobi. His research focuses on the investigation of molecular thin films by tip-enhanced Raman spectroscopy.

The real part of the dielectric functions of metals show an overall decrease from small positive values (below 1) in the UV to negative values in the visible and infrared part of the electromagnetic spectrum, as predicted by the optical response of the free electrons in the conduction band (classical Drude model).[12,22,23] As mentioned above, this allows for plasmon resonances to occur at frequencies that are specific for each metal [depending on $\mathrm{Re}(\varepsilon(\omega))$]. The actual magnitude of the polariton resonance is determined by $\mathrm{Im}(\varepsilon(\omega))$, which ideally should have a value close to zero (see above), because then dissipation losses are minimal.[12] The dielectric function of different metals can be found in various textbooks[12,24,25] and their evaluation leads to the conclusion that the highest resonances can be expected for Ag and Au in the visible range (typical wavelength range for Raman spectroscopic measurements). Silver and gold are indeed most frequently used as materials for optical probes.[26] Interband transitions stretching from the near-UV to the visible region are the most pronounced difference between the dielectric function of Au compared to the one from Ag. Consequently, Au (similar to Cu) has a significant optical absorption below about 600 nm (high value for the imaginary part of the dielectric function in this range), but can exhibit strong resonances above 600 nm. In contrast, Ag is suitable for plasmonics over the whole visible range. Other metals such as platinum, palladium, and aluminum strongly absorb in the whole visible range. Aluminum is, however, suitable for applications with UV excitation.[27,28] The above-mentioned condition and the trend of the real part of the metals dielectric function also implies that an increase in the dielectric constant ε_M of the surrounding medium leads to a red-shift of the localized surface plasmon resonance. This effect was used by Yeo et al.[29] and recently also by Hayazawa et al.[30] to tune the resonance frequency of a near-field optical probe to the blue/green spectral range by changing the underlying tip material in direct contact with the enhancing silver structure to a low-refractive-index material (e.g. SiO_x, AlF_3).

The resonance frequency of the localized surface plasmon resonance is independent of the size of the sphere as long as the electrostatic approximation holds true. For larger spheres (best described by the Mie solution to the Maxwell equations), a red-shift of the resonance is observed as the particle size increases. The resonance condition can become very complicated when particle geometries other than a perfect sphere are considered. Extending the above theory for small spherical particles to small ellipsoidal particles leads to a modified resonance condition with the possibility of up to three distinct extinction peaks (the absorption depends on the incident polarization).[25] In the case of polarization along the longer axis of a spheroid, a red-shift of the resonance is expected with increasing aspect ratio. One approach which uses this phenomenon in the design of a tunable near-field probe was recently reported in the literature.[31] Fleischer et al. placed gold nanocones on AFM cantilevers as efficient optical probes. By varying the height of the gold cones (accompanied by a shift in their resonance wavelength), Fleischer et al. were able to adapt their optical probes to a large part of the visible spectrum (500–700 nm). Despite the large range of necessary heights (10–170 nm), the tip radius at the apex stayed the same, thus allowing for highly localized fields over the whole spectral range. For further details on the concentration of light by plasmonic structures, we refer to the recent review by Schuller et al.[32]

Localized surface plasmon resonances are considered to be the main contribution to the observed field enhancement, but other effects (mainly geometrical) can also contribute to the field enhancement. For example, "field line crowding" at any sharp tip apex can lead to a nonresonant local field enhancement independent of the excitation wavelength (lightning rod effect).[33] Correlations of the local field enhancement with, for example, the tip length and the apex radius of a silicon probe (to have no contribution from polaritons) were presented in a theoretical study by Esteban et al.[34] It was shown that a smaller apex radius leads to a more confined field and increased scattering. Furthermore, it was pointed out that very small tips (or even spheres) produce more confined fields than the long tips typically used for apertureless SNOM studies. Esteban et al. also discussed antenna-like resonances, which have to be considered when evaluating the tip length. This effect, known from traditional antenna theory, can also be used to specifically design efficient near-field optical probes.[35]

Carolin Blum studied chemistry at the Karlsruhe Institute of Technology, Germany, and received her diploma in 2010. Since 2011 she has been carrying out PhD research at the ETH Zurich, Switzerland, under the supervision of Prof. Renato Zenobi. Her research concentrates on the comparison of tip-enhanced Raman scattering with other Raman methods and the investigation of biological samples by tip-enhanced Raman spectroscopy.

Renato Zenobi studied chemistry at the ETH Zurich (MSc 1986) and completed his PhD at Stanford University (USA) in 1990. After postdoctoral research at the Universities of Pittsburgh and Michigan, he moved to the EPFL, Lausanne in 1992 as a Werner Fellow, where he established his own research group. He became assistant professor at the ETH in 1995, associate professor in 1997, and full professor in 2000. His research includes laser-based analytical chemistry, mass spectrometry, and scanning microscopy as well as the development of analytical methods for the nanoscale, in particular tip-enhanced Raman spectroscopy.

3. Technical Issues To Be Considered for TERS Imaging

3.1. Fear of Contact: Tip–Sample Distance

An STM or AFM feedback scheme is normally used to control the tip–sample separation during TERS imaging experiments. When an STM technique is used, the distance control is based on the tunneling current between the tip and a conductive substrate, which is a strictly monotonic (decreasing) function of the tip–sample distance. The insulating gap is typically in the range of 0.5–1 nm. When an AFM technique is used, the distance control is based on forces acting between tip and sample surface, which cannot be described by a monotonic function (depending on the distance, repulsive or attractive forces dominate). When operated in contact mode, the tip–sample separation is typically smaller than in STM feedback control (< 0.5 nm), which can be a considerable advantage (higher field enhancement), but can also lead, for example, to displacement or pick-up of sample molecules. Other feedback schemes sometimes used for TERS are tapping/semicontact mode AFM[36–39] and shear force feedback using a tuning fork.[40–42]

The local field strength at the sample surface decays rapidly with increasing tip–sample separation. This phenomenon is a very good indicator of a true near-field effect. A recent study by Yano et al.[43] evaluated the effect of varying the tip–sample distance in tip-enhanced Raman experiments. They used a silver-coated silicon AFM probe in tapping-mode feedback. By using a time-gated photon-counting scheme, the detected Raman signal could be correlated with the vertical distance between the tip and the sample surface over the range of the tapping amplitude. They found an exponential decay of the near-field Raman intensity with increasing tip–sample separation, with typical values at $1/e$ between 10 and 25 nm depending on the tip used.

Other studies state that the TER intensity (and the TER background intensity) is inversely proportional to the tenth power of the tip–sample distance. In most cases, no near-field contribution was observed for distances larger than 20 nm.[44–51]

3.2. TERS by Numbers: Contrast, Enhancement Factor, and Field Confinement

The so-called enhancement factor is regularly used to compare different TERS studies, despite the high variability of enhancement factors cited in the literature.[52,53] The motivation to use an enhancement factor mainly stems from single-molecule TERS, where it is applied to estimate whether the enhancement is sufficient to detect single molecules at all. In TERS imaging experiments, however, reducing the near-field enhancement effects to a single number does not have much practical value. Characteristics such as spectroscopic contrast, field confinement, and the far-field-illuminated area/volume are of much higher practical relevance when considering TERS imaging experiments, because they give a direct measure of the achievable image quality (resolution, contrast) and the necessary collection time.

The spectroscopic contrast can be determined by performing a "tip-in–tip-out experiment" (Figure 2a), where the Raman peak intensity with the enhancing tip in contact with the sample surface is directly compared to the peak intensity on the sample surface with the tip in a retracted position. The most common definition is given by Equation (1)[26,53–55]

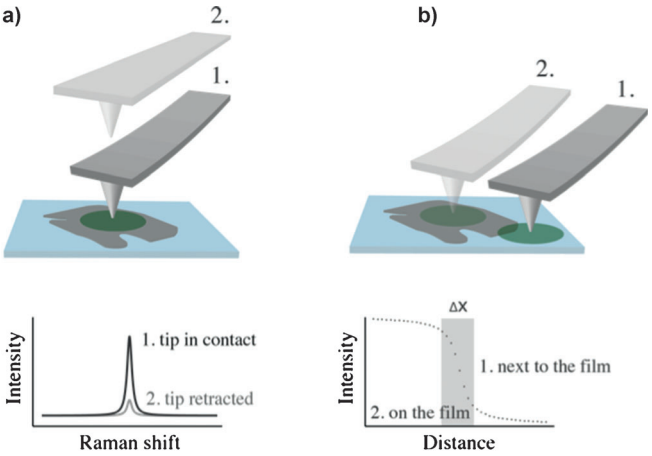

Figure 2. Schematic illustration of the experimental procedure for determining the contrast (a) and the lateral field confinement (b). To determine the spectroscopic contrast, the Raman band intensity with the enhancing tip in contact with the sample surface (a, 1) is directly compared to the peak intensity on the sample surface with the tip in a retracted position (a, 2). A line scan across the edge of a thin film (e.g. graphene) from a position next to the film (b, 1) to a position on the film (b, 2) shows an intensity slope, where Δx is a direct measure for the lateral extent of the near-field contribution (if the far-field contribution is negligible). The green circle symbolizes the size of the laser focus spot.

$$\gamma = \frac{I_{nf}}{I_{ff}} = \frac{I_{tip-in} - I_{tip-out}}{I_{tip-out}} = \frac{I_{tip-in}}{I_{tip-out}} - 1 \quad (1)$$

where $I_{tip\text{-}in}$ is the Raman signal intensity when the near-field probe is in contact with the sample, $I_{tip\text{-}out}$ is the Raman signal intensity at the same sample position with the tip retracted, I_{nf} is the pure near-field signal intensity, and I_{ff} the (pure) far-field signal intensity.

The field confinement mainly depends on the probe dimensions, and distance curves give a good idea of the near-field nature of the enhancement and the field confinement in the z direction (see Section 3.1). The lateral field confinement can be most practically determined by a line scan across a sharp edge of a thin film of a strong Raman scatterer (e.g. graphene): the resolution is directly connected to the distance Δx (Figure 2b) over which the intensity increases from 10% to 90% of the final Raman intensity (on the film), which simply corresponds to the full width at half maximum (FWHM) of the line-spread function (first derivative of the edge response). A one-dimensional structure such as a single-

walled carbon nanotube can also be used, where the near-field confinement directly corresponds to the measured intensity profile across the tube.[56]

The far-field illuminated area should also be mentioned in the context of tip-enhanced Raman imaging, because it can have a considerable impact on the outcome of an imaging experiment. Continuous irradiation of a large sample area should be avoided to prevent photoinduced sample decomposition or bleaching. Considering a 128×128 pixel near-field image with a pixel size of 10 nm for a typical TERS imaging experiment, the investigated area of 1.64 μm^2 is almost seven times larger than the area illuminated by a tightly focused excitation laser beam in a bottom illumination TERS experiment, when an oil-immersion objective can be used. In a typical side-illumination TERS experiment, the area that is continuously illuminated by the excitation laser may be close to 2 μm^2, which may lead to much more sample damage if the same power density is used. Recent TERS approaches without direct far-field illumination of the sample are, therefore, of particular interest for imaging experiments.[17,20]

3.3. What a Spectrum Can Tell: Interpretation of TERS Data

TERS peaks have to be assigned correctly and their existence or absence as well as their intensities have to be brought into the right context to ensure a reasonable interpretation. At the moment, the most commonly used way to assign bands in a TER spectrum is to compare them to available SERS or conventional Raman data in the literature.[26] Recently, a study by Blum et al. has revealed how SER, gap-mode TER, and conventional Raman spectra of amino acids, peptides, and proteins actually compare (all measured on the same instrument). Key findings were that the band positions are identical with all three methods (except for modes that are directly affected by interactions with the substrate or, more generally, by changes of bonds or the molecular structure), but the intensity ratios can vary dramatically.[57] In addition, it was observed that fewer bands are present in TER than in confocal Raman spectra and that TERS seems to be closer to SERS than to conventional Raman spectroscopy in this respect.

It was also pointed out recently by Stadler et al. that if individual peaks are assigned by comparing them with enough literature data, and allowing for a tolerance in band position of a few cm^{-1}, almost any possible peak assignment can be obtained.[26] We therefore propose that, when being solely dependent on reference data from the literature, the spectral positions of the observed fingerprint bands should be compared as a *set* to the corresponding reference spectrum to ascertain that the peak patterns match well.

The observed variations in band intensity ratios may be related, for example, to a lowering of the symmetry through an interaction with the substrate or tip,[58] a possible (but still not experimentally proven) influence of a field gradient effect,[59] or the strongly enhanced and localized electromagnetic field that is present in a plasmonically coupled system, such as, in the so-called gap-mode STM configuration.[26] In addition, the orientation of the molecule with respect to the polarization of the laser beam is also important, as is known from conventional Raman spectroscopy.[58,60]

Care has to be taken, too, when comparing TER spectra measured on different setups. This is due to several factors: a standardization method is missing that takes into account that the technical specifications and the spectrometer calibrations differ from instrument to instrument. This issue is already well-known in the Raman community,[61] and a standardization method for comparing conventional Raman spectra obtained on different instruments has been proposed by Rodriguez et al.[62] Such a procedure would be highly beneficial for the TERS community as well.

For interpretation of TERS data, we propose to build up a spectral database for SERS, TERS, and conventional Raman spectroscopy data, comparable to already existing databases such as the NIST Chemistry WebBook. In such a database the spectra should be standardized with respect to the instrumental parameters, and the most important experimental conditions of the TERS experiments should be clearly stated. Such a database would be a big help to the community, as it would allow data to be assigned and compared much more easily and reliably.

3.4. Tip Contamination: On Parasitic Spectra and Spurious Bands

It is already well-known that carbon contaminations can be produced by, for example, sample heating.[59,63] For long measurement times (in the range of minutes) their Raman signals often average to two broad bands (D and G band) centered around 1350 cm^{-1} and 1580 cm^{-1}, respectively, which can be easily recognized.[59] Nevertheless, these broad background signals do not necessarily obscure the spectrum of the intact material, as this often can be identified easily as sharp Raman bands superimposed on the broad background signals. Kudelski and Pettinger,[64] Bjerneld et al.,[65] Pieczonka and Aroca,[66] Moyer et al.,[67] and Richards et al.[68] have also discussed such carbon contaminations for SERS and TERS.

Furthermore, TER (and SER) spectra often show a broadband background which is not related to carbon contaminations and whose origin is not yet fully understood. Inelastic scattering from the metallic nanostructures present on the tip apex, enhanced fluorescence, and plasmon-coupled emissions have been cited as possible causes.[69–75] The most common explanation is that a plasmon-dependent photoluminescence from the rough metal surface (or from the tip–sample gap)[46] accounts for the background. Molecular fluorescence is expected to be quenched by electronic coupling to the metal surface/tip and can probably be excluded as a source of the observed broad background signal.[46]

Other sources for parasitic spectra are silver oxides, sulfides, and related species formed in the reaction of the tip surface with atmospheric compounds. Most noticeable are two modes at around 220–240 cm^{-1}, which have been assigned to molecular oxygen chemisorbed on defect sites.[66,76]

If contamination leads to strong and sharp peaks that resemble peaks from the spectral fingerprint of the analyte, it is much harder to recognize these peaks as contamination

signals. Possibilities to examine whether the observed spectrum belongs to a parasitic substance or not are, for example, to thoroughly compare the spectral pattern to Raman spectroscopy or SERS data (see Section 3.3) or to perform a time-dependent measurement, as contamination signals often fluctuate. For example, carbon contaminations can lead to a distinct spectral pattern of sharp peaks typically above 1000 cm^{-1} whose intensities vary with time.[26,46,59,77–80] Chaigneau et al. and Domke et al. discussed the appearance of such fluctuating signals in the context of single-molecule detection with TERS.[59,77]

Spectral fluctuation, however, is a matter of the applied timescale. Figure 3 shows a typical example. An electrochemically etched silver tip was dipped into a thiophenol solution, brought into STM feedback with a clean gold substrate, and spectra with one-second integration time were collected successively. The two black spectra in Figure 3a show how the TER spectra of thiophenol look throughout the major part of this measurement. For comparison we show a stronger TER spectrum of thiophenol (in green) which was collected by using a longer integration time. However, not only could signals originating from the analyte itself be observed, but also two kinds of spectra (red and blue), which show a distinct and reproducible pattern over 19 s and 28 s, respectively (Figure 3b,c). Even though they are relatively stable over this time period, a comparison with the analyte spectrum reveals that they result from parasitic contaminations, for example, from sample degradation or from material that was picked up by the tip or that diffused into the probed volume. If one performs an experiment with many different substances present in the sample (e.g. biological samples) it can easily happen that a contamination fairly consistently produces a spectrum that might look like the "complex" spectra one would expect. When performing an imaging experiment, a strong hint for such a contamination is that the parasitic spectra often appear only in one line of an area scan. One can in such a case repeat the measurement with a different tip, or scan forwards and backwards on the same line and see if the same spectral features are observed. The tip can also be tested on an empty substrate or a spectrum can be measured with the excitation laser focused on the retracted tip to rule out tip contamination.

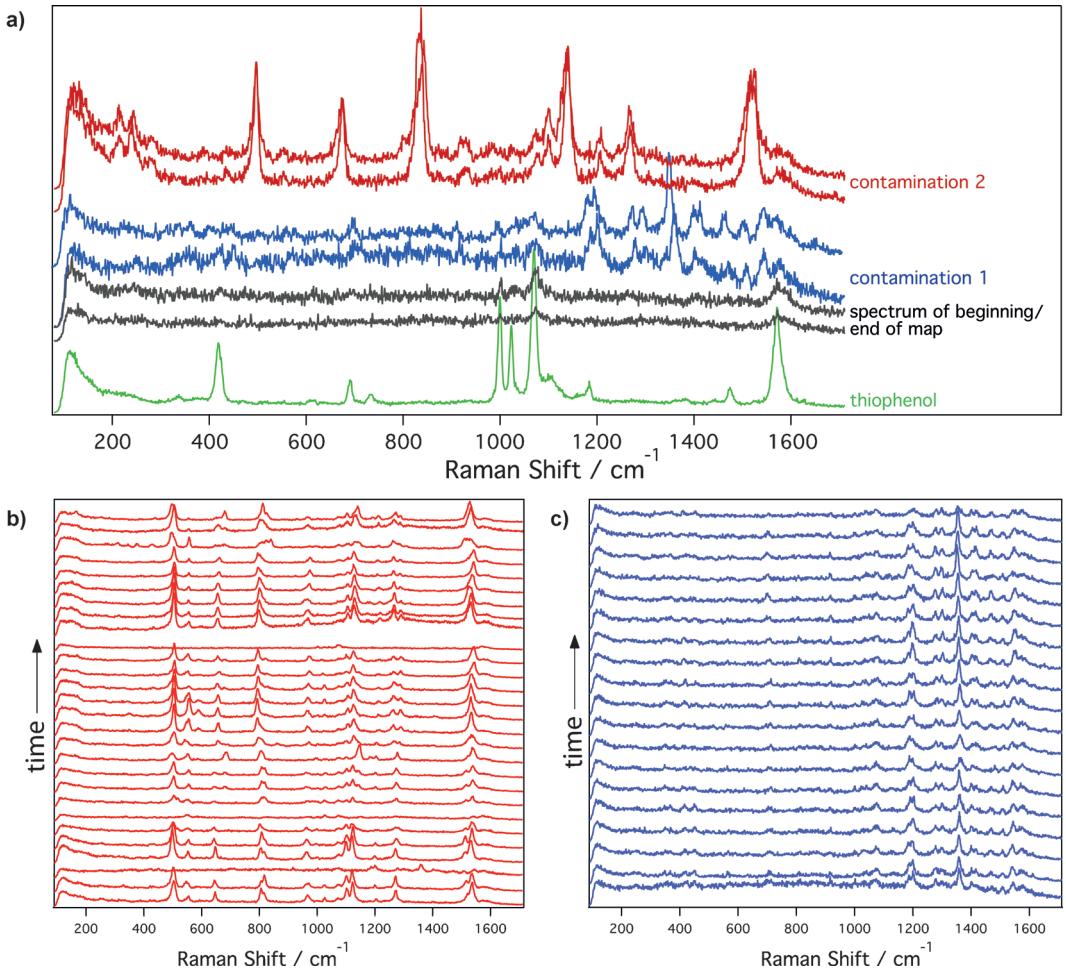

Figure 3. a) Black: Thiophenol spectrum at the beginning/end of the measurement. Blue/red: Examples of contamination spectra. Green: Stronger TER spectrum of thiophenol, recorded using a longer measurement time. b) Time-dependent evolution of the spectra of contamination 2. c) Time-dependent evolution of the spectra of contamination 1. Integration time: 1 s per spectrum. The spectra are displaced vertically for better visibility.

3.5. Lifetime of a Tip: Chemical and Mechanical Degradation

The high reactivity of nanorough silver tips is considered a possible reason for fast chemical degradation of the tip over time.[81] Reactions of silver with oxygen or sulfur compounds from the atmosphere alter the surface plasmon resonance and typically lead to a vanishing of the enhancement within 24 h.[81] One can extend the tip lifetime by using gold tips, but there is a trade-off of less enhancement. For weak Raman scatterers, in particular, this is often not an option.

Mechanical degradation of the tip can occur through a change in the shape of the nanostructure at the very end of the tip, which causes a change in TERS intensity.[82] As the most commonly used TERS tips consist of the rather ductile materials gold or silver (comapared to, e.g., silicon nitride) full metal tips, in particular, can be deformed during an imaging experiment.[63] Metal-coated AFM tips can lose parts of the coating as the metal might not adhere strongly enough to the underlying tip material.

Another source of tip degradation that is well known in the literature results from heating through the laser illumination, which can induce changes in shape and morphology of the nanostructure. For a general overview we refer to the review by Yeo et al. (see the section on "nearfield heating")[63] and the one by Stadler et al. (see the section on "local heating").[26] Interestingly, it was shown by several research groups that it is possible to shield the enhancing nanoparticle from such heating effects by a protective coating. The first results for SERS particles were reported, for example, by John et al.[83] and Whitney et al.[84] However, experimentally, a protective layer has until now always resulted in a reduced enhancement as the distance between the enhancing particle and the analyte molecules is increased.

3.6. The Drowned Tip: Performing TERS in Liquids

Most TERS experiments have so far been performed on solid samples at atmospheric pressure,[26] and some in ultra-high vacuum.[52,85–87] Certain—for example, biological—samples are only stable in water or buffer solutions, and for studying chemical reactions or adsorption processes it could even be of interest to work in organic solvents. There has been only one proof-of-principle study so far where TERS was carried out in liquids.[88] The study revealed difficulties and proposed solutions to overcome them. For example, the tip coating has to be robust enough not to peel off in a liquid environment. It was shown that a two-layer coating of SiO_x ($x = 1$–2) and Ag on silicon nitride AFM probes is mechanically sufficiently stable for experiments in water.[88] In contrast to the tip coating, feedback mechanisms for controlling the tip–sample distance in a liquid environment are commercially available: modern AFMs are often equipped for operation in liquids or even come with a sealed liquid cell. It was found when studying a self-assembled monolayer of thiophenol on a thin Au film immersed in water with these Ag-SiO_x-coated AFM tips that tip contamination is critical when performing TERS in liquids. Sample molecules can adsorb to the tip coating, which itself acts as a SERS substrate. Finally, adsorbates can be decomposed into carbonaceous species by the laser irradiation. To overcome this problem, the tip surface needs to be protected against contamination. Self-assembled monolayers of thiols are known to replace carbon contamination on SERS-active Ag surfaces[89] and have been successfully applied as protective layers on Ag-coated AFM tips for TERS in water.[88]

Conducting a TERS experiment in water also has a practical advantage: It was found experimentally that immersing the TERS tip in or covering a SERS substrate with water significantly reduces fluctuating carbon signals.[88] Finally, when performing a TERS experiment in a liquid environment, one has to consider the effect on the surface plasmon resonance frequency of the enhancing tip. As mentioned in Section 2, an increase in the refractive index around the enhancing metal shifts the plasmon resonance to longer wavelengths. Thus, a red-shift is expected when a TERS tip is immersed in water.

3.7. A Picture Is Worth a Thousand Spectra: TERS Imaging

Tip-enhanced Raman imaging provides spectroscopic contrast, for example, to visualize the distribution of organic molecules on a sample surface[90] or to map physical stress on inorganic crystal lattices[39] on the nanometer scale. It delivers basically the same spectroscopic information as confocal Raman imaging; however, by introducing a near-field optical probe a considerably higher spatial resolution can be achieved. Some additional restrictions arising from the presence of the SPM probe are added: because the enhanced electromagnetic field at the tip apex decreases rapidly with increasing tip–sample distance (see Section 3.1), tip-enhanced Raman imaging is restricted to the uppermost layer of a sample surface. Furthermore, as the tip is normally fixed in position relative to the focused laser beam and only the sample is moved during an imaging experiment, the maximum image size and scan speed for a TERS imaging experiment is determined by the positioning system of the sample stage (typically piezoelectric scanners).

It is known from confocal Raman imaging that, as a consequence of the inherently low Raman cross-section of most sample molecules, the collection, transfer, and detection of the scattered light has to be as efficient as possible to allow short acquisition times. The same holds true for TERS imaging. One aspect that contributes to the overall efficiency of a TERS imaging experiment is the detector used. However, since electron-multiplying CCD cameras with single-photon detection capabilities are available, sufficient detector sensitivity is often not a big issue anymore.

Recent TERS imaging studies with acquisition of full spectra in every pixel demonstrated that a spatial resolution of about 10 nm can be achieved and acquisition times of 50 ms/pixel are possible for strong Raman scatterers[90,91] and 500 ms/pixel for weak Raman scatterers.[92,93] These studies include images with up to 256×256 pixels. If a pixel size of 5 nm (chosen below the expected spatial resolution of 10–20 nm) is used, the largest area that can be scanned at 50 ms/pixel in 1 h has a size of $1.34 \times 1.34\ \mu m^2$. Typical values for the

thermal drift of a state-of-the-art atomic force microscope are in the range of 0.01–0.1 nm s^{-1}, i.e., the total drift during a 1 h imaging experiment is between 36 and 360 nm. Direct comparison of these values to the estimated maximum scan area of $1.34 \times 1.34\ \mu m^2$ immediately shows that thermal drift can have a significant influence on the resulting image quality. Additionally, when the excitation laser has a typical focal spot diameter in the range of 300 to 2000 nm (depending on the laser wavelength and the used objective), the whole imaged sample area or a large fraction of it is illuminated during the entire imaging experiment. This can limit the total imaging time because of possible photodegradation of sample molecules.

As the Raman signal intensity is proportional to the amount of analyte inside the measurement volume, quantitative measurements with TERS are theoretically possible, but they are hampered by the effects that other parameters have on the signal intensity, such as fluctuations in the laser power and TERS contrast during a measurement (for example, because of instabilities in the tip–sample distance). Temporal changes in the AFM or STM feedback lead to fluctuations of the TERS contrast, which in TERS images manifest themselves as lines of higher or lower enhancement that are parallel to the scan direction of the tip, and thus are very similar to artifacts known from AFM and STM. An example for this can be seen in Section 4.4 in Figure 7a and b, where the enhancement in a line in the lower part was significantly higher than in the upper part of the image. A simple way to correct for that was shown recently: Opilik et al. and Stadler et al.[92,94] used the ratio between two characteristic marker bands (from two different compounds) instead of their absolute values to obtain the corresponding image. In this way it was possible to achieve a uniform distribution (see Figure 7c).[94] Another approach is to use an internal standard such as, for example, the tip material itself (Ichimura et al. used the Si peak of their tip as an internal standard)[95] or an additional coating (e.g. a self-assembled monolayer of a thiol) whose Raman signal intensity is used to monitor changes in the enhancement and/or laser power during a TERS experiment. Bortchagovsky et al. and Schmid et al. independently mentioned this idea,[88,96] and its realization is a part of ongoing research.

4. Applications of TERS Imaging in Materials and Life Sciences

4.1. Nano in 1D: Nanotubes and Nanowires

Conventional Raman spectroscopy is widely used to characterize quasi-one-dimensional structures such as carbon nanotubes, to give fundamental insight into their optical and electronic properties.[97] However, the optical imaging of their nanoscale properties is severely restricted due to the optical diffraction limit. Tip-enhanced Raman spectroscopy was soon recognized as a perfect tool to overcome this limitation, and has been extensively used since 2003 to investigate such one-dimensional structures (not only carbon nanotubes but also, e.g., CdSe nanowires). The research groups of Novotny,[40,44,98] Hartschuh,[45,99–103] Maultzsch,[104–106] Williams,[107] and Kawata[11,108] have made significant contributions in this area. Carbon nanotubes have also become a popular "test sample" for new technical developments in TERS, for example, in the study of Weber-Bargioni et al.[91] to test new nanofabricated coaxial antenna tips and in the study by Roy and Williams[107] with radially polarized laser beams. In the following we highlight two different applications of TERS on carbon nanotubes that in our eyes are exemplary for how much the technique has already matured.

Peica et al. showed that TERS can be used to localize different single-walled carbon nanotubes within a carbon nanotube bundle.[109] They investigated the topography and the TER spectra at several positions along a small bundle and observed varying contributions from the different radial breathing modes. By correlating these changes and the changes in the G^- mode with the height profile of the bundle they were able to state which nanotube was present at which position in the bundle. This is a good illustration of how TERS can be used to gain information that otherwise would not have been accessible, as either the chemical or the topographical information would have been missing.

Yano et al. studied the TER spectra of single-walled carbon nanotubes in situ while they increased the pressure applied by their tip (pressure assisted TERS).[11] They investigated a semiconducting[11] and a metallic[110] nanotube, respectively. They showed that the G mode of the nanotube shifts by as much as 10 cm^{-1} on increasing the pressure (Figure 4). The electronic properties of the nanotube were found to determine whether it is both the low- and the high-frequency (semiconducting) peak that contribute to the G band, or only the high-frequency mode (metallic) that is shifted. The different behavior is related to the fact that the semiconducting nanotubes are chiral and the vibrational directions of these modes are not purely circumferential compared to the low- and high-frequency modes of metallic nanotubes. Additionally, they used pressure-assisted TERS to prove that one-dimensional imaging with a spatial resolution of about 4 nm is possible; this results from the small contact area the pressure-applying tip shares with the nanotube.

4.2. Nano in 2D: Graphene

The studies by Novoselov, Geim et al.[111,112] (Nobel Prize in Physics in 2010) on one-layer-thick graphite (graphene), generated by peeling off layer by layer from graphite flakes by adhesive tape, paved the way for a large number of studies on this unique material. The properties of graphene suggest many potential applications, for example, in field-effect transistors, memory devices, as transparent electrodes, and as light absorbers in photovoltaic devices.[113] For all these applications, nanoanalytical tools are needed to characterize the graphene in terms of size, shape, electronic properties, and distribution of defects and contaminants.

The most intense bands in the Raman spectra of both graphite and graphene are the G band at about 1580 cm^{-1} and the 2D band at about 2700 cm^{-1}. Furthermore, defects give

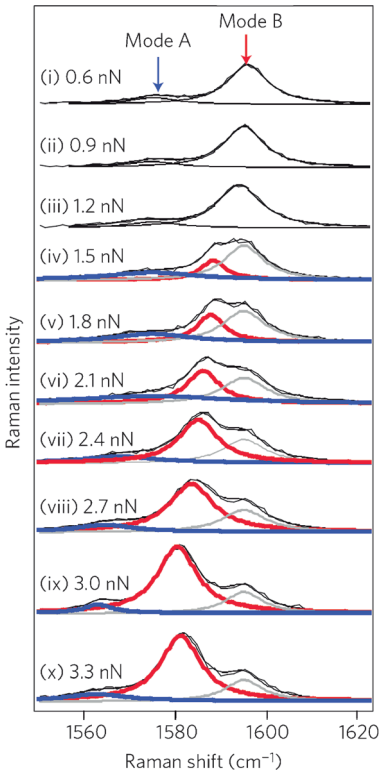

Figure 4. Sensing of a slight local deformation in a single-walled nanotube (SWNT) as a result of tip-applied pressure by means of Raman spectroscopy. The TERS spectra of a SWNT in the G-band range, comprising mode A (blue curves) and mode B (red curves), show significant dependence on the tip-applied force. (Reproduced with permission from *Nature Photonics*, Ref. [11]. Copyright 2009, Macmillan Publishers Limited.)

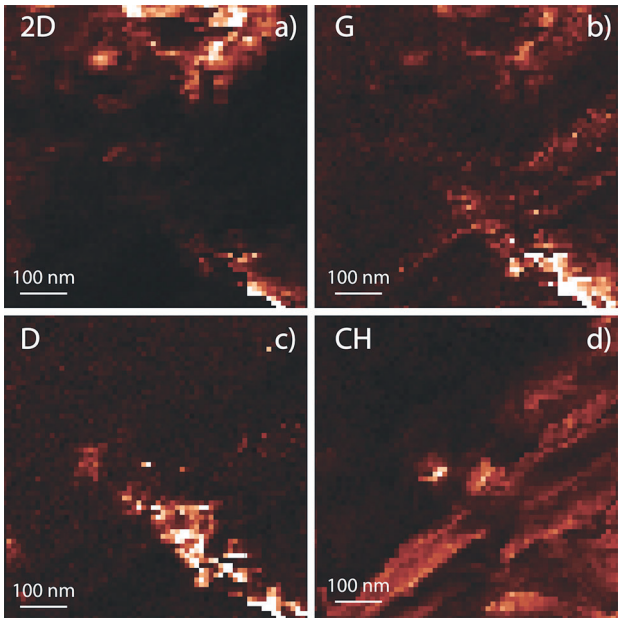

Figure 5. Raman image of graphene on Cu (64×64 pixels, 640×640 nm^2, 0.25 s per spectrum). Background and enhancement-corrected band intensities of the a) 2D band at 2634 cm^{-1} typical for single-layer graphene, b) graphene G band at 1580 cm^{-1}, c) D band at 1350 cm^{-1}, and d) CH stretching modes at 2800–3000 cm^{-1}. The TERS maps show the clear localization of graphene defects (c) and the complementary behavior of the 2D (a) and CH bands (d). (Adapted from Ref. [118].)

rise to a D band at 1350 cm^{-1}.[114] In 2008, the first TER spectra showing the G, D, and 2D bands of graphene were obtained by Hoffmann and Loos by using an inverted-microscope TERS scheme.[115] Soon after, Domke and Pettinger[116] used side-illumination STM-TERS to investigate graphene grown on 6H-SiC and found weak enhancement of the SiC bands and even weaker enhancement of the graphene bands. They explained this observation by the ineffective coupling of the near field that is oriented parallel to the tip with graphene modes that vibrate parallel to the sample surface and, therefore, perpendicular to the tip axis. Saito et al.[117] performed a TERS line scan on a stack of five graphene layers across steps down to a single layer in an inverted-microscope configuration and found a decrease in the G band intensity and an intense D band at edges and defects. Snitka et al.[55] presented novel gold cantilevers fabricated by flattening gold microwires and electrochemical etching of nanotips and their use in obtaining enhanced Raman spectra of graphene. In their experiments, they found tip-pressure-induced changes to the 2D band.

The first 2D TERS maps of graphene were performed by Stadler et al.[118] in 2011 (Figure 5). A top-illumination STM-TERS setup allowed the investigation of single-layer graphene prepared by the adhesive-tape technique on gold and of commercially available graphene produced by chemical vapor deposition (CVD) on copper without any additional sample preparation. The images revealed the distribution of graphene and defects with a lateral resolution of < 12 nm. As in the work of Domke and Pettinger,[116] in-plane modes such as the G band were only weakly enhanced, because of their orientation perpendicular to the tip. This has the advantage that defects, folds, contaminants, and in general deviations from the two-dimensional structure of pristine graphene can be detected with high specificity and sensitivity above the "background" signals of pristine graphene. For this reason, previously unobserved Raman signals that can be assigned to hydrogen-terminated graphene or hydrocarbon contaminations have been detected by TERS on CVD-produced graphene which are not detectable by normal confocal Raman spectroscopy. TERS maps with up to 100×100 pixels show the distribution of graphene, defects, and H-terminated/contaminated areas. As a result of the strong enhancement (contrast of up to 80), 32×32 pixel images were recorded in as few as 5 min.[118]

4.3. Nanoheterogeneous Thin Films: Solar Cell Materials

Most photovoltaic (PV) devices used nowadays are based on crystalline silicon (c-Si) solar cells, but there is a growing research field that searches for more cost-efficient alternatives. The main idea is to find thin-film solar cell absorbers (hundreds of nanometers to a few micrometers film thickness) that need much less material than bulk absorbers, that can be

produced at normal atmospheric conditions, and that achieve conversion efficiencies almost as high as bulk c-Si cells. The two main thrusts of this research deal with chalcopyrite-type inorganic materials, such as $CuInS_2$ (CIS), $CuInSe_2$ (CISe), and $Cu(In,Ga)Se_2$ (CIGSe), as well as organic photovoltaics (OPV), such as polymer blends of poly(3-hexylthiophene) (P3HT) and [6,6]-phenyl-C_{61}-butyric acid methyl ester (PCBM). The conversion efficiency of CIGSe thin-film solar cells is already relatively close to the efficiency of c-Si cells, with record values of 19.6% and 25.0%, respectively.[119] Organic solar cells have reached conversion efficiencies of up to 10.0%,[119] and their efficiencies are still rapidly increasing (by a factor of 3 over the last 10 years).[120] Challenges for chemical analysis arise from the lateral and depth heterogeneities at the micro- and nanometer scale within these thin-film materials.

A pioneering combined confocal Raman and SNOM study of a P3HT:PCBM sample by Klimov et al. in 2006[121] was followed by a study by Zhang et al. in 2009–2010,[122,123] who used a parabolic mirror-based TERS setup for chemical imaging of this material. TERS and tip-enhanced photoluminescence (PL) are ideal tools, because their spatial resolution of ≤ 9 nm matches the exciton diffusion length in P3HT (8.5 ± 0.7 nm).[124] The tip-enhanced spectra of a P3HT:PCBM model system show a Raman band at 1450 cm^{-1} attributed to the C=C stretching vibration of P3HT as well as PL emission from PCBM and P3HT, respectively. Mapping experiments revealed that the two polymers are not perfectly segregated, as was concluded from islands with sizes in the upper nanometer to lower micrometer range that are clearly visible in shear-force AFM topography images of this material. P3HT was distributed all over the thin film—although very inhomogeneously—and the islands exhibit higher amounts of PCBM. From the ratio of the P3HT photoluminescence (depending on both PL activity and concentration of P3HT) and Raman signal intensity (depending only on the P3HT concentration), the authors were able to draw conclusions about the local PL quenching efficiency, which is known to be a measure of electron transport from the P3HT donor to the PCBM acceptor molecules and was found to be high in the PCBM-enriched islands. Finally, tip-enhanced spectroscopy helped in understanding the influence of different annealing times on the micro- and nanostructure of these model polymer blends (Figure 6).[123] More recently, Zhang et al. investigated 30 nm thin films of the organic semiconductor diindoperylene (DIP), which also resulted in tip-enhanced PL emission and tip-enhanced Raman scattering of the material, thus underlining the general applicability of the method to organic semiconductors/photovoltaics.[125]

Chalcopyrite-type thin-film solar cell absorbers, such as the CIS/CISe/CIGS/CIGSe system, consist of layers that add up to a few micrometers in thickness and contain heterogeneities along the depth axis, such as concentration gradients, stress, and strain, which have been studied at the micro- and nanometer scale.[126] Compared to other methods used in this field, such as X-ray fluorescence analysis (XRF), Raman spectroscopy has the advantage of delivering information about the stoichiometry and crystal structure of the materials instead of merely elemental information.[127] Therefore, TERS of cross-sectional samples of thin-film solar cell materials should yield interesting information about such inorganic materials. This would have to be performed in a top-illumination/top-detection setup because of the opacity of the materials. Tools for the chemical analysis of thin-film solar cell materials at the micro- and nanometer scale are definitively needed, because there are still many remaining questions concerning the relationship between fabrication/processing, micro- and nanostructure, and solar cell efficiency. The potential of tip-enhanced spectroscopy for studying single surface states in inorganic semiconductors, such as Nb-doped rutile (TiO_2), has recently been demonstrated by Sevinc et al.[128]

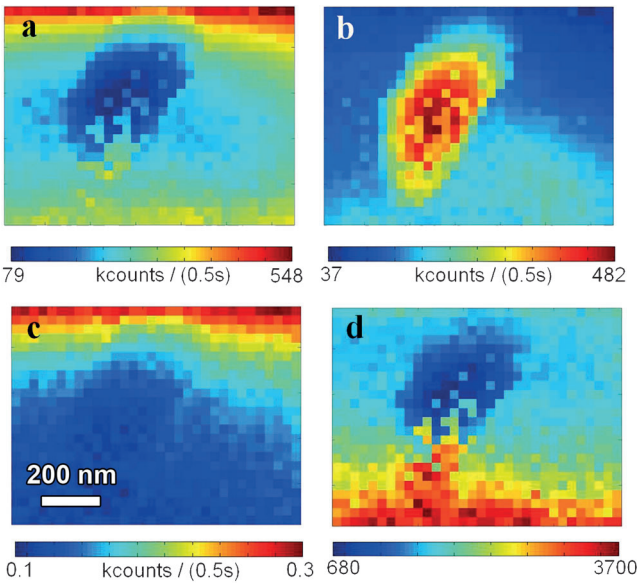

Figure 6. Photoluminescence intensity distribution of P3HT (a), PCBM (b), and ν(C=C) Raman intensity (c) of P3HT on a P3HT:PCBM blend film. d) P3HT photoluminescence quenching efficiency in the same scan area (pixel-by-pixel ratio of the values from (a) and (c)). Scan area: 1 μm × 0.75 μm, 32 × 28 pixels. (Adapted from Ref. [123] with permission.)

4.4. Just a Few Molecules: Patterned Self-Assembled Monolayers of Thiols

For some applications, for example, in catalysis or biology, the chemical characterization of molecules on a surface is crucial for understanding their reactivity and function. However, the small quantity of molecules present render their spectroscopic characterization challenging.

An example of how TERS can map the distribution of a few analyte molecules on surfaces—even if they have very similar chemical structures—was given by Stadler et al. in their study on patterned thiol monolayers (Figure 7).[94] It succeeded an earlier study on TERS imaging of thiols by Picardi et al., who investigated the influence of the STM parameters and the polarization of the incident laser beam on the signal of an azobenzene thiol monolayer.[93] Stadler et al. microcontact printed circles of 2-mercaptopyridine (2-PySH)

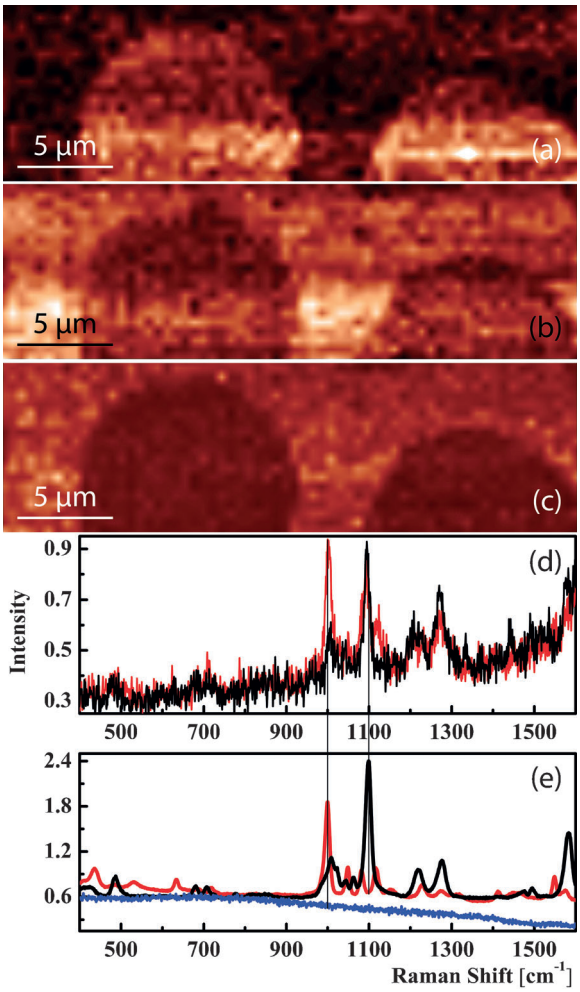

Figure 7. a)–c) Tip-enhanced spectroscopic images; 30×10 μm^2. a) Intensity of the 2-PySH marker band at 1000 cm^{-1}. b) Intensity of the 4-PySH marker band at 1100 cm^{-1}. The images show complementary patterns with higher intensity of the microcontact-printed thiol in the circles and higher intensity of the thiol used to fill the gaps around the circular areas. c) Intensity ratio of the two marker bands. d) TERS spectra (0.5 s) from the printed 2-PySH area (red) and the area covered with 4-PySH (black). Small residues of 4-PySH in the red curve are visible at 1100 cm^{-1}. e) Reference SERS spectra (120 s) from 2-PySH (red) and SERS spectrum (10 s) of 4-PySH (black) and a confocal background spectrum (60 s; blue) from a 2-PySH thiol monolayer. (Adapted from Ref. [94].)

on an ultraflat gold substrate and filled the spaces between the circles by immersing the sample into a solution of isomeric 4-mercaptopyridine (4-PySH). When the sample was characterized by AFM (topography, phase contrast), it was not possible to distinguish the different regions. Furthermore, it was not possible to obtain any signals by confocal Raman spectroscopy, because these thiols are only weak Raman scatterers and the number of molecules in the laser focus was too small. However, it was possible to detect and distinguish the two isomers with TERS imaging. Stadler et al. used an electrochemically etched silver tip in the so-called gap-mode configuration and scanned it over the sample while measuring a full Raman spectrum at each pixel by using low laser powers (300 μW) and short acquisition times (0.5 s). The 30×10 μm^2 images show the intensities of the respective marker bands of the two isomeric thiols (Figure 7 a,b). The resulting complementary pattern of the two thiols (2-PySH in the circles and 4-PySH surrounding it) is in agreement with the pattern of the microcontact stamp that was used to prepare the sample. This experiment demonstrates the usefulness of TERS, as its enhancement and the spectroscopic information in every pixel of the image is needed to characterize this sample. However, the lateral resolution provided by TERS was not fully exploited (one pixel was 500 nm).

4.5. Rafting at the Nanoscale: Mixed Supported Lipid Layers

TERS imaging on biological samples is a challenging but also very promising task. The nanometer-scale resolution of TERS imaging in combination with the enhancement effects make it possible to image weakly scattering small biological molecules. It was recently shown by Opilik et al. that it is possible to use TERS imaging to investigate lipid domains (Figure 8).[92] These lipid domains caused by the phase separation of the different lipid compounds are believed to be good model systems to study the compartmentalization of biological membranes into lipid rafts. Opilik et al. used the Langmuir–Blodgett technique to deposit a monolayer of a binary mixture containing a saturated and an unsaturated phospholipid onto an ultraflat gold substrate. To reveal the lateral distribution of the individual components in this supported lipid monolayer, they used an electrochemically

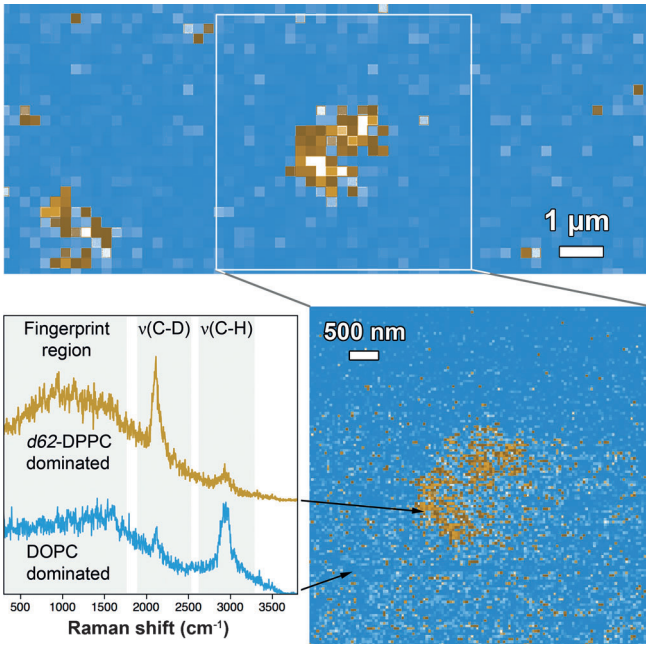

Figure 8. TERS imaging of a mixed lipid monolayer deposited onto gold by the Langmuir–Blodgett technique. The map of the band intensity ratios of ν(C-D) (marker band of *d*62-DPPC) and ν(C–H) reveals domains that are dominated by the saturated lipid *d*62-DPPC and are surrounded by areas dominated by the unsaturated lipid DOPC. (Adapted from Ref. [92].) The color scale is chosen arbitrarily.

etched silver tip to perform gap-mode STM-TERS. The dominant C–H stretching vibrations in the Raman spectrum (commonly used as lipid marker bands)[129] were chosen to visualize the distribution of the two lipids. For clear spectroscopic differentiation, the saturated lipid was replaced by its deuterated (*d*62) equivalent. The resulting C–D modes appear at lower wavenumbers and could easily be distinguished from the C–H modes of the undeuterated (unsaturated) lipid. In a first step, Opilik et al. used a TERS overview scan of 6×15 μm to localize a lipid domain of interest and then imaged this domain in a high-resolution image of 128×128 pixels (each with full spectral information in every pixel) with a step size of 47 nm—well below the optical diffraction limit. The measurement time was as low as 0.5 s per pixel at a laser power of only 300 μW. To obtain the images, Opilik et al. plotted the intensity ratio of the two marker bands to remove image artifacts, as described in Section 3.7. These TERS images nicely show the phase segregation of the two lipids in domains enriched in the saturated lipid surrounded by the fluid phase mainly consisting of the unsaturated lipid.

5. Summary and Outlook

In recent years, TERS has developed into a powerful spectroscopic imaging technique for the uppermost surface layer (typically the first 10–20 nm) of modern materials and biological systems. The exceptional high spatial resolution combined with the spectroscopic information makes TERS a unique tool to look at the nanoworld. However, the technique still faces some technological challenges, which are related to the enhancing tip and mainly concern the extent and reproducibility of the enhancement, spatial resolution, and tip lifetime. The basic principles of tip enhancement that are important for the improvement of TERS probes are discussed in Section 2.

The use of TERS for imaging experiments gives rise to technical issues that go beyond the optimization of the enhancing tip and are discussed in Section 3. Some of these important aspects are: 1) TERS probes are still fabricated by the end user according to individual recipes with low tip-to-tip reproducibility. Direct comparison of TERS results from different probes is, therefore, only possible if key figures such as contrast and lateral resolution are reported. Methods for their determination are described in Section 3.2. 2) Interpretation of TERS data includes careful band assignment as well as the identification of parasitic spectra arising from contamination of the tip. This is particularly challenging for biological samples, because of their highly heterogeneous (and often only partly known) composition and their sensitivity to photodegradation. Guidelines for band assignment and identification of parasitic spectra are given in Sections 3.3 and 3.4. The compilation of a TERS/SERS/Raman database would be a very helpful tool in this context and first efforts in this direction are being made. 3) Collection times per pixel have to be reduced as much as possible to avoid mapping times of several hours and the distortion of images because of the intrinsic drift of the SPM. Thus, strongly enhancing tips, highly efficient optical systems, and CCD cameras are needed (see Section 3.7). 4) Customized software and hardware integration of SPM and Raman instruments is fundamental for performing fully automated TERS imaging experiments. 5) Temporal and/or local changes in the enhancement during a mapping experiment lead to measurement artifacts, and strategies for their removal are discussed in Section 3.7.

The selected applications of TERS imaging reviewed in Section 4 highlight the potential of this technique for the characterization of nanomaterials, such as nanotubes, nanowires, and graphene, as well as novel thin-film solar cell materials. In some cases, it is not the high spatial resolution that makes TERS an interesting tool for surface analysis: the extraordinary enhancement allows the identification of only a few molecules from self-assembled monolayers and to image their distribution on a larger scale (see Section 4.4). As shown exemplarily in Section 4.5 for a mixed supported lipid layer, TERS imaging on a nanometer length scale has the potential to yield new insight into biological systems.

We can conclude that only 12 years after its first description in the literature, TERS is definitely coming of age. Several companies are now making serious efforts to build and possibly market TERS systems. In the SPM industry, TERS is viewed as a value-generating addition to STM and AFM, where markets may be stagnating. The promise of TERS is clearly the possibility to provide chemical identification on the nanometer scale, which is viewed as a crucial element in its application in chemistry, materials science, and biology.

We gratefully acknowledge Bruker Corp. (Bruker Nano Surfaces Division) for collaboration and financial support. We thank Johannes Stadler (ETH Zurich) for critical discussions and providing data for Figure 3. Dr. Dai Zhang (University of Tübingen) is acknowledged for providing Figure 6. C.B. thanks the Stiftung Stipendien-Fonds des Verbandes der chemischen Instustrie e.V. (funding) and the German National Academic Foundation for scholarships.

Received: May 18, 2012
Revised: September 2, 2012
Published online: April 22, 2013

[1] A. Engel, *Adv. Imaging Electron Phys.* **2009**, *159*, 357 – 386.
[2] I. Medalsy, U. Hensen, D. J. Muller, *Angew. Chem.* **2011**, *123*, 12309 – 12314; *Angew. Chem. Int. Ed.* **2011**, *50*, 12103 – 12108.
[3] S. W. Hell, *Science* **2007**, *316*, 1153 – 1158.
[4] S. Berning, K. I. Willig, H. Steffens, P. Dibaj, S. W. Hell, *Science* **2012**, *335*, 551.
[5] J. C. Vaughan, X. Zhuang, *Nat. Biotechnol.* **2011**, *29*, 880 – 881.
[6] G. T. Dempsey, J. C. Vaughan, K. H. Chen, M. Bates, X. Zhuang, *Nat. Methods* **2011**, *8*, 1027 – 1036.
[7] R. M. Stöckle, Y. D. Suh, V. Deckert, R. Zenobi, *Chem. Phys. Lett.* **2000**, *318*, 131 – 136.
[8] N. Hayazawa, Y. Inouye, Z. Sekkat, S. Kawata, *Opt. Commun.* **2000**, *183*, 333 – 336.
[9] M. S. Anderson, *Appl. Phys. Lett.* **2000**, *76*, 3130 – 3132.
[10] B. Pettinger, G. Picardi, R. Schuster, *Electrochemistry* **2000**, *68*, 942 – 949.
[11] T. Yano, P. Verma, Y. Saito, T. Ichimura, S. Kawata, *Nat. Photonics* **2009**, *3*, 473 – 477.

[12] E. C. Le Ru, P. G. Etchegoin, *Principles of Surface-Enhanced Raman Spectroscopy and Related Plasmonic Effects*, Elsevier, New York, **2009**.
[13] E. H. Synge, *Philos. Mag.* **1928**, *6*, 356 – 362.
[14] D. W. Pohl, W. Denk, M. Lanz, *Appl. Phys. Lett.* **1984**, *44*, 651 – 653.
[15] A. Lewis, M. Isaacson, A. Harootunian, A. Muray, *Ultramicroscopy* **1984**, *13*, 227 – 231.
[16] L. Neumann, Y. Pang, A. Houyou, M. L. Juan, R. Gordon, N. F. van Hulst, *Nano Lett.* **2011**, *11*, 355 – 360.
[17] S. Berweger, J. M. Atkin, R. L. Olmon, M. B. Raschke, *J. Phys. Chem. Lett.* **2010**, *1*, 3427 – 3432.
[18] F. Keilmann, R. Hillenbrand, *Philos. Trans. R. Soc. London Ser. A* **2004**, *362*, 787 – 806.
[19] M. B. Raschke, C. Lienau, *Appl. Phys. Lett.* **2003**, *83*, 5089 – 5091.
[20] F. De Angelis, G. Das, P. Candeloro, M. Patrini, M. Galli, A. Bek, M. Lazzarino, I. Maksymov, C. Liberale, L. C. Andreani, E. Di Fabrizio, *Nat. Nanotechnol.* **2010**, *5*, 67 – 72.
[21] L. Novotny, B. Hecht, *Principles of Nano-Optics*, Cambridge University Press, Cambridge, **2006**.
[22] P. Drude, *Ann. Phys.* **1900**, *306*, 566 – 613.
[23] P. Drude, *Ann. Phys.* **1900**, *308*, 369 – 402.
[24] E. D. Palik, *Handbook of Optical Constants of Solids III*, Academic Press, New York, **1998**.
[25] C. F. Bohren, D. R. Huffman, *Absorption and Scattering of Light by Small Particles*, Wiley, New York, **1983**.
[26] J. Stadler, T. Schmid, R. Zenobi, *Nanoscale* **2012**, *4*, 1856 – 1870.
[27] Z. Yang, Q. Li, Y. Fang, M. Sun, *Chem. Commun.* **2011**, *47*, 9131 – 9133.
[28] A. Taguchi, N. Hayazawa, K. Furusawa, H. Ishitobi, S. Kawata, *J. Raman Spectrosc.* **2009**, *40*, 1324 – 1330.
[29] B.-S. Yeo, T. Schmid, W. Zhang, R. Zenobi, *Anal. Bioanal. Chem.* **2007**, *387*, 2655 – 2662.
[30] N. Hayazawa, T. Yano, S. Kawata, *J. Raman Spectrosc.* **2012**, *43*, 1177 – 1182.
[31] M. Fleischer, A. Weber-Bargioni, M. V. P. Altoe, A. M. Schwartzberg, P. J. Schuck, S. Cabrini, D. P. Kern, *ACS Nano* **2011**, *5*, 2570 – 2579.
[32] J. A. Schuller, E. S. Barnard, W. Cai, Y. C. Jun, J. S. White, M. L. Brongersma, *Nat. Mater.* **2010**, *9*, 193 – 204.
[33] A. Ermushev, B. V. Mchedlishvili, V. Oleĭnikov, A. Petukhov, *Quantum Electron.* **1993**, *23*, 435 – 440.
[34] R. Esteban, R. Vogelgesang, K. Kern, *Nanotechnology* **2006**, *17*, 475 – 482.
[35] L. Novotny, N. van Hulst, *Nat. Photonics* **2011**, *5*, 83 – 90.
[36] N. Marquestaut, D. Talaga, L. Servant, P. Yang, P. Pauzauskie, F. Lagugné-Labarthet, *J. Raman Spectrosc.* **2009**, *40*, 1441 – 1445.
[37] Y. Ogawa, T. Toizumi, F. Minami, A. Baranov, *Phys. Rev. B* **2011**, *83*, 081302.
[38] B. R. Wood, E. Bailo, M. A. Khiavi, L. Tilley, S. Deed, T. Deckert-Gaudig, D. McNaughton, V. Deckert, *Nano Lett.* **2011**, *11*, 1868 – 1873.
[39] P. Hermann, M. Hecker, D. Chumakov, M. Weisheit, J. Rinderknecht, A. Shelaev, P. Dorozhkin, L. M. Eng, *Ultramicroscopy* **2011**, *111*, 1630 – 1635.
[40] N. Anderson, A. Hartschuh, L. Novotny, *Nano Lett.* **2007**, *7*, 577 – 582.
[41] C. Williams, D. Roy, *J. Vac. Sci. Technol. B* **2008**, *26*, 1761 – 1764.
[42] S. Kharintsev, G. Hoffmann, P. Dorozhkin, J. Loos, *Nanotechnology* **2007**, *18*, 315502.
[43] T.-A. Yano, T. Ichimura, A. Taguchi, N. Hayazawa, P. Verma, Y. Inouye, S. Kawata, *Appl. Phys. Lett.* **2007**, *91*, 121101.
[44] L. G. Cançado, A. Jorio, A. Ismach, E. Joselevich, A. Hartschuh, L. Novotny, *Phys. Rev. Lett.* **2009**, *103*, 186101.
[45] M. Böhmler, A. Hartschuh, *ChemPhysChem* **2012**, *13*, 927 – 929.
[46] C. C. Neacsu, S. Berweger, M. B. Raschke, *Nanobiotechnology* **2007**, *3*, 172 – 196.
[47] C. C. Neacsu, J. Dreyer, N. Behr, M. B. Raschke, *Phys. Rev. B* **2006**, *73*, 193406.
[48] L. Novotny, S. J. Stranick, *Annu. Rev. Phys. Chem.* **2006**, *57*, 303 – 331.
[49] B. Pettinger, K. F. Domke, D. Zhang, R. Schuster, G. Ertl, *Phys. Rev. B* **2007**, *76*, 113409.
[50] R. M. Roth, N. C. Panoiu, M. M. Adams, R. M. Osgood, C. C. Neacsu, M. B. Raschke, *Opt. Express* **2006**, *14*, 2921 – 2931.
[51] B. Pettinger, K. F. Domke, D. Zhang, G. Picardi, R. Schuster, *Surf. Sci.* **2009**, *603*, 1335 – 1341.
[52] B. Pettinger, P. Schambach, C. J. Villagómez, N. Scott, *Annu. Rev. Phys. Chem.* **2012**, *63*, 379 – 399.
[53] T. Schmid, B. S. Yeo, W. Zhang, R. Zenobi, *Tip Enhancement* (Eds.: S. Kawata, V. M. Shalaev), Elsevier, Amsterdam, **2007**.
[54] C. A. Barrios, A. V. Malkovskiy, A. M. Kisliuk, A. P. Sokolov, M. D. Foster, *J. Phys. Chem. C* **2009**, *113*, 8158 – 8161.
[55] V. Snitka, R. D. Rodrigues, V. Lendraitis, *Microelectron. Eng.* **2011**, *88*, 2759 – 2762.
[56] D. Roy, J. Wang, C. Williams, *J. Appl. Phys.* **2009**, *105*, 013530.
[57] C. Blum, T. Schmid, L. Opilik, S. Weidmann, S. R. Fagerer, R. Zenobi, *J. Raman Spectrosc.* **2012**, *43*, 1895 – 1904.
[58] J. R. Lombardi, R. L. Birke, *J. Phys. Chem. C* **2008**, *112*, 5605 – 5617.
[59] K. F. Domke, D. Zhang, B. Pettinger, *J. Phys. Chem. C* **2007**, *111*, 8611 – 8616.
[60] X. Gao, J. P. Davies, M. J. Weaver, *J. Phys. Chem.* **1990**, *94*, 6858 – 6864.
[61] R. L. McCreery, *Raman Spectroscopy for Chemical Analysis*, Wiley, New York, **2000**.
[62] J. D. Rodriguez, B. J. Westenberger, L. F. Buhse, J. F. Kauffman, *Analyst* **2011**, *136*, 4232 – 4240.
[63] B.-S. Yeo, J. Stadler, T. Schmid, R. Zenobi, W. Zhang, *Chem. Phys. Lett.* **2009**, *472*, 1 – 13.
[64] A. Kudelski, B. Pettinger, *Chem. Phys. Lett.* **2000**, *321*, 356 – 362.
[65] E. J. Bjerneld, F. Svedberg, P. Johansson, M. Käll, *J. Phys. Chem. A* **2004**, *108*, 4187 – 4193.
[66] N. P. W. Pieczonka, R. F. Aroca, *ChemPhysChem* **2005**, *6*, 2473 – 2484.
[67] P. J. Moyer, J. Schmidt, M. Lukas, A. J. Meixner, G. W. Sandmann, H. Dietz, W. Plieth, *J. Am. Chem. Soc.* **2000**, *122*, 5409 – 5410.
[68] D. Richards, R. Milner, F. Huang, F. Festy, *J. Raman Spectrosc.* **2003**, *34*, 663 – 667.
[69] J. Heritage, J. Bergman, A. Pinczuk, J. Worlock, *Chem. Phys. Lett.* **1979**, *67*, 229 – 232.
[70] T. Itoh, V. Biju, M. Ishikawa, Y. Kikkawa, K. Hashimoto, A. Ikehata, Y. Ozaki, *J. Chem. Phys.* **2006**, *124*, 134708.
[71] J. Jiang, K. Bosnick, M. Maillard, L. Brus, *J. Phys. Chem. B* **2003**, *107*, 9964 – 9972.
[72] S. Mahajan, R. M. Cole, J. D. Speed, S. H. Pelfrey, A. E. Russell, P. N. Bartlett, S. M. Barnett, J. J. Baumberg, *J. Phys. Chem. C* **2010**, *114*, 7242 – 7250.
[73] Y. Maruyama, M. Futamata, *Chem. Phys. Lett.* **2005**, *412*, 65 – 70.
[74] M. Moskovits, *J. Raman Spectrosc.* **2005**, *36*, 485 – 496.
[75] A. Otto, J. Timper, T. Billmann, G. Kovacs, I. Pockrand, *Surf. Sci.* **1980**, *92*, L55 – L57.
[76] G. I. N. Waterhouse, G. A. Bowmaker, J. B. Metson, *Appl. Surf. Sci.* **2003**, *214*, 36 – 51.
[77] M. Chaigneau, G. Picardi, R. Ossikovski, *Surf. Sci.* **2010**, *604*, 701 – 705.
[78] B.-S. Yeo, E. Amstad, T. Schmid, J. Stadler, R. Zenobi, *Small* **2009**, *5*, 952 – 960.

[79] W. Zhang, T. Schmid, B. S. Yeo, R. Zenobi, *J. Phys. Chem. C* **2008**, *112*, 2104 – 2108.
[80] J. Tsang, J. Demuth, P. Sanda, J. Kirtley, *Chem. Phys. Lett.* **1980**, *76*, 54 – 57.
[81] C. Barrios, A. Malkovskiy, R. Hartschuh, *Proc. SPIE* **2008**, *6954*, 69540C.
[82] B.-S. Yeo, T. Schmid, W. Zhang, R. Zenobi, *Appl. Spectrosc.* **2008**, *62*, 708 – 713.
[83] J. F. John, S. Mahurin, S. Dai, M. J. Sepaniak, *J. Raman Spectrosc.* **2010**, *41*, 4 – 11.
[84] A. V. Whitney, J. W. Elam, P. C. Stair, R. P. Van Duyne, *J. Phys. Chem. C* **2007**, *111*, 16827 – 16832.
[85] J. Steidtner, B. Pettinger, *Rev. Sci. Instrum.* **2007**, *78*, 103104.
[86] N. Jiang, E. T. Foley, J. M. Klingsporn, M. D. Sonntag, N. A. Valley, J. A. Dieringer, T. Seideman, G. C. Schatz, M. C. Hersam, R. P. Van Duyne, *Nano Lett.* **2012**, 12, 5061 – 5067.
[87] J. Steidtner, B. Pettinger, *Phys. Rev. Lett.* **2008**, *100*, 236101.
[88] T. Schmid, B.-S. Yeo, G. Leong, J. Stadler, R. Zenobi, *J. Raman Spectrosc.* **2009**, *40*, 1392 – 1399.
[89] K. L. Norrod, K. L. Rowlen, *Anal. Chem.* **1998**, *70*, 4218 – 4221.
[90] J. Stadler, T. Schmid, R. Zenobi, *Nano Lett.* **2010**, *10*, 4514 – 4520.
[91] A. Weber-Bargioni, A. Schwartzberg, M. Cornaglia, A. Ismach, J. J. Urban, Y. Pang, R. Gordon, J. Bokor, M. B. Salmeron, D. F. Ogletree, S. Cabrini, P. J. Schuck, *Nano Lett.* **2011**, *11*, 1201 – 1207.
[92] L. Opilik, T. Bauer, T. Schmid, J. Stadler, R. Zenobi, *Phys. Chem. Chem. Phys.* **2011**, *13*, 9978 – 9981.
[93] G. Picardi, M. Chaigneau, R. Ossikovski, C. Licitra, G. Delapierre, *J. Raman Spectrosc.* **2009**, *40*, 1407 – 1412.
[94] J. Stadler, T. Schmid, L. Opilik, P. Kuhn, P. S. Dittrich, R. Zenobi, *Beilstein J. Nanotechnol.* **2011**, *2*, 509 – 515.
[95] T. Ichimura, H. Watanabe, Y. Morita, P. Verma, S. Kawata, Y. Inouye, *J. Phys. Chem. C* **2007**, *111*, 9460 – 9464.
[96] E. G. Bortchagovsky, U. C. Fischer, *J. Raman Spectrosc.* **2009**, *40*, 1386 – 1391.
[97] M. S. Dresselhaus, G. Dresselhaus, R. Saito, A. Jorio, *Phys. Rep.* **2005**, *409*, 47 – 99.
[98] A. Hartschuh, H. Qian, C. Georgi, M. Böhmler, L. Novotny, *Anal. Bioanal. Chem.* **2009**, *394*, 1787 – 1795.
[99] L. G. Cançado, A. Hartschuh, L. Novotny, *J. Raman Spectrosc.* **2009**, *40*, 1420 – 1426.
[100] A. Hartschuh, E. J. Sánchez, X. S. Xie, L. Novotny, *Phys. Rev. Lett.* **2003**, *90*, 95503.
[101] A. Hartschuh, N. Anderson, L. Novotny, *J. Microsc.* **2003**, *210*, 234 – 240.
[102] C. Georgi, A. Hartschuh, *Appl. Phys. Lett.* **2010**, *97*, 143117.
[103] M. Böhmler, Z. Wang, A. Myalitsin, A. Mews, A. Hartschuh, *Angew. Chem.* **2011**, *123*, 11740 – 11742; *Angew. Chem. Int. Ed.* **2011**, *50*, 11536 – 11538.
[104] N. Peica, S. Röhrig, A. Rüdiger, K. Brose, C. Thomsen, J. Maultzsch, *Phys. Status Solidi B* **2009**, *246*, 2708 – 2712.
[105] K. Goß, N. Peica, C. Thomsen, J. Maultzsch, C. M. Schneider, C. Meyer, *Phys. Status Solidi B* **2011**, *248*, 2577 – 2580.
[106] N. Peica, C. Thomsen, J. Maultzsch, *Phys. Status Solidi B* **2010**, *247*, 2818 – 2822.
[107] D. Roy, C. Williams, *J. Vac. Sci. Technol. A* **2010**, *28*, 472 – 475.
[108] A. Tarun, N. Hayazawa, T. A. Yano, S. Kawata, *J. Raman Spectrosc.* **2011**, *42*, 992 – 997.
[109] N. Peica, C. Thomsen, J. Maultzsch, *Nanoscale Res. Lett.* **2011**, *6*, 174.
[110] T.-A. Yano, Y. Inouye, S. Kawata, *Nano Lett.* **2006**, *6*, 1269 – 1273.
[111] K. S. Novoselov, *Science* **2004**, *306*, 666 – 669.
[112] K. S. Novoselov, D. Jiang, F. Schedin, T. J. Booth, V. V. Khotkevich, S. V. Morozov, A. K. Geim, *Proc. Natl. Acad. Sci. USA* **2005**, *102*, 10451 – 10453.
[113] X. Huang, Z. Yin, S. Wu, X. Qi, Q. He, Q. Zhang, *Small* **2011**, *7*, 1876 – 1902.
[114] A. Ferrari, J. Meyer, V. Scardaci, C. Casiraghi, M. Lazzeri, F. Mauri, S. Piscanec, D. Jiang, K. Novoselov, S. Roth, *Phys. Rev. Lett.* **2006**, *97*, 187401.
[115] G. G. Hoffmann, J. Loos, *Macromol. Symp.* **2008**, *265*, 1 – 11.
[116] K. F. Domke, B. Pettinger, *J. Raman Spectrosc.* **2009**, *40*, 1427 – 1433.
[117] Y. Saito, P. Verma, K. Masui, Y. Inouye, S. Kawata, *J. Raman Spectrosc.* **2009**, *40*, 1434 – 1440.
[118] J. Stadler, T. Schmid, R. Zenobi, *ACS Nano* **2011**, *5*, 8442 – 8448.
[119] M. A. Green, K. Emery, Y. Hishikawa, W. Warta, E. D. Dunlop, *Prog. Photovoltaics Res. Appl.* **2012**, *20*, 12 – 20.
[120] P. G. Nicholson, F. A. Castro, *Nanotechnology* **2010**, *21*, 492001.
[121] E. Klimov, W. Li, X. Yang, G. Hoffmann, J. Loos, *Macromolecules* **2006**, *39*, 4493 – 4496.
[122] D. Zhang, X. Wang, K. Braun, H. J. Egelhaaf, M. Fleischer, L. Hennemann, H. Hintz, C. Stanciu, C. J. Brabec, D. P. Kern, *J. Raman Spectrosc.* **2009**, *40*, 1371 – 1376.
[123] X. Wang, D. Zhang, K. Braun, H. J. Egelhaaf, C. J. Brabec, A. J. Meixner, *Adv. Funct. Mater.* **2010**, *20*, 492 – 499.
[124] P. E. Shaw, A. Ruseckas, I. D. W. Samuel, *Adv. Mater.* **2008**, *20*, 3516 – 3520.
[125] D. Zhang, U. Heinemeyer, C. Stanciu, M. Sackrow, K. Braun, L. E. Hennemann, X. Wang, R. Scholz, F. Schreiber, A. J. Meixner, *Phys. Rev. Lett.* **2010**, *104*, 056601.
[126] D. Abou-Ras, R. Caballero, C. H. Fischer, C. A. Kaufmann, I. Lauermann, R. Mainz, H. Mönig, A. Schöpke, C. Stephan, C. Streeck et al., *Microsc. Microanal.* **2011**, *17*, 728 – 751.
[127] T. Schmid, C. Camus, S. Lehmann, D. Abou-Ras, C. H. Fischer, M. C. Lux-Steiner, R. Zenobi, *Phys. Status Solidi A* **2009**, *206*, 1013 – 1016.
[128] P. C. Sevinc, X. Wang, Y. Wang, D. Zhang, A. J. Meixner, H. P. Lu, *Nano Lett.* **2011**, *11*, 1490 – 1494.
[129] C. W. Freudiger, W. Min, B. G. Saar, S. Lu, G. R. Holtom, C. He, J. C. Tsai, J. X. Kang, X. S. Xie, *Science* **2008**, *322*, 1857 – 1861.